Characterization of a commercial PEM fuel cell stack by means of physics–based modeling and distribution of relaxation times

Andrei Kulikovsky[a)]
Forschungszentrum Jülich GmbH
Theory and Computation of Energy Materials (IEK–13)
Institute of Energy and Climate Research,
D–52425 Jülich, Germany

(Dated: 31 January 2022)

Impedance spectra of a commercial Polymer Electrolyte Membrane Fuel Cell (PEMFC) stack are analyzed by means of fitting a physics–based model and distribution of relaxation times (DRT) techniques. Oxygen transport coefficients of the gas–diffusion layer, cathode catalyst layer (CCL), and the CCL proton conductivity are determined for the stack current densities of 150, 250 and 400 mA cm^{-2}. DRT function returns reaction resistivity and transport resistivites of the channel and porous layers. A good agreement between the transport parameters resulting from the fitted model and DRT is demonstrated.

Keywords: PEM fuel cell stack, impedance, DRT, modeling

I. INTRODUCTION

To increase output power PEM fuel cells are assembled in stacks. Typical PEMFC stack consists of ten to hundred tightly clamped cells fed through manifolds for hydrogen and air supply. An important task in PEMFC technology is regular stack testing and characterization to prevent failures due to degradation of transport or kinetic parameters.

Electrochemical impedance spectroscopy (EIS) is a non–invasive and non–destructive tool best suited for stack testing. Theoretically, impedance spectrum of a stack contains complete information on oxygen transport coefficients in porous layers, on kinetics of oxygen reduction reaction (ORR) and so on. However, extraction of this information from the spectrum requires rather sophisticated modeling (see reviews[1,2]). So far, simple equivalent circuits (ECs) have been used to recover mean transport parameters from the stack spectra[3–7]. Drawbacks of this approach are well known: any EC is not unique and even EC with the impedance spectrum close to the spectrum of interest may give misleading results[8]. Another approach is establishing indicators of stack fault behavior using frequency plots of impedance module and phase angle[9].

A relatively new technique of spectra analysis is distribution of relaxation times (DRT)[10,11]. This technique attracts growing interest of PEM fuel cell community and several works have been devoted to analysis of single cell DRT[12–15]. However, to the best of our knowledge, so far DRT of a stack has not been calculated and analyzed.

In this work, our physics–based model for PEMFC impedance is extended to stack level. The model is fitted to recently published experimental spectra of a commercial Ballard stack[16]. Further, we calculate distribution of relaxation times (DRT) functions from the experimental and fitted model impedance spectra. The DRT spectra are calculated using a novel K_2 kernel, which better captures low– and medium–frequency transport processes in a PEM fuel cell as compared to the classic Debye kernel[17].

DRT spectra of a Ballard stack at the current densities of 150, 250 and 400 mA cm^{-2} exhibit five peaks. We attribute the peaks (in ascending frequency order) to (1) oxygen transport in the channel, (2) oxygen transport in the GDL, (3) oxygen reduction reaction, and (4,5) proton transport in the catalyst layer. A contribution of every process to the total cell resistance is calculated and the respective transport parameters are estimated. Parameters resulted from the fitted model and DRT analysis are compared and discussed.

II. PHYSICS–BASED IMPEDANCE MODEL

The model for single cell impedance is described in detail in[18,19]. Here, we briefly outline the basic model equations. The transient mass– and charge–transport equations which form the basis for impedance model are shown in Figure 1. To describe variation of oxygen concentration along the straight cathode channel the cell is separated into N virtual segments. In every segment, oxygen transport in the gas–diffusion layer (GDL) and the cathode catalyst layer (CCL) is described by the diffusion equations. Proton charge conservation equation in the CCL completes the system (Figure 1). The right side of equations in the CCL is the Tafel rate of the ORR. Oxygen transport equation in the channel "links" segments providing the boundary condition for the through–plane oxygen transport (Figure 1).

Transient equations in Figure 1 are linearized and Fourier–transformed leading to a system of linear equations for the small overpotential η^1 and oxygen c^1 perturbation amplitudes. This system is solved for every segment and the local (segment) impedance Z_{seg} is calculated according to

$$Z_{seg} = -\left.\frac{\eta^1}{\sigma_p \partial\eta^1/\partial x}\right|_{x=0} \qquad (1)$$

The segments are connected in parallel and the cell

a)Electronic mail: A.Kulikovsky@fz-juelich.de

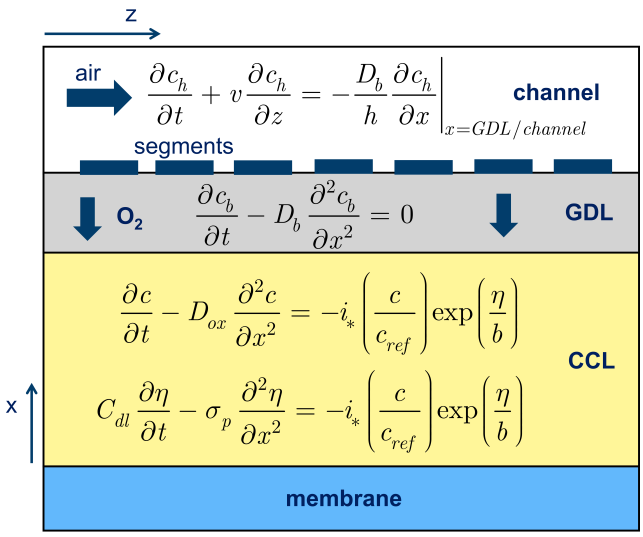

FIG. 1. Basic transient transport equations for a single cell in the stack. For notations see Nomenclature section.

impedance Z_{cell} is calculated from equation

$$\frac{1}{Z_{cell}} = \frac{1}{N}\sum_{n=1}^{N}\frac{1}{Z_{seg}} \tag{2}$$

Finally, impedance of a stack with M cells Z_{stack} is a sum of cell impedances

$$Z_{stack} = \sum_{m=1}^{M} Z_{cell,m} \tag{3}$$

where the subscript m enumerates cells.

Chang et al.[20] compared measured and model variation of air flow distribution along the manifold feeding the cell cathodes in a stack and reported a parabolic–like 10% decay of the flow velocity. This decay has been modeled as the parabolic 10%–decay of stoichiometry

$$\lambda = \lambda^0\left(0.95 + 0.1\cdot\left(1-\tilde{y}^2\right)\right), \quad 0 \le \tilde{y} \le 1 \tag{4}$$

where λ^0 is the air (oxygen) flow stoichiometry at the manifold inlet and $\tilde{y}$ is the distance along the manifold normalized to the manifold length.

III. DRT ANALYSIS

In this work, K_2 kernel was used for DRT calculation[17]. With this kernel, the basic DRT equation has the form

$$Z(\omega) = R_\infty + R_{pol}\int_{-\infty}^{\infty}\frac{\tanh\left(\alpha\sqrt{\mathrm{i}\omega\tau}\right)G(\tau)\,d\ln(\tau)}{\alpha\sqrt{\mathrm{i}\omega\tau}\,(1+\mathrm{i}\omega\tau)} \tag{5}$$

where α is a step function of the frequency $f = \omega/(2\pi)$

$$\alpha = 1 - H(f - f_*) + \epsilon, \tag{6}$$

$H(x)$ is the Heaviside step function and $\epsilon = 10^{-10}$ is a small parameter to avoid zero division error. Parameter α changes from 1 to 0 at the threshold frequency $f = f_*$. Compared to the standard Debye kernel $1/(1+\mathrm{i}\omega\tau)$, Eq.(5) contains the Warburg finite–length factor $\tanh\left(\alpha\sqrt{\mathrm{i}\omega\tau}\right)/\left(\alpha\sqrt{\mathrm{i}\omega\tau}\right)$. With $\alpha \to 0$, this factor tends to unity:

$$\frac{\tanh\left(\alpha\sqrt{\mathrm{i}\omega\tau}\right)}{\alpha\sqrt{\mathrm{i}\omega\tau}} \to 1, \quad \text{as} \quad \alpha \to 0 \tag{7}$$

and hence at the frequencies above f_*, the K_2 kernel reduces to the standard Debye kernel. Eq.(5) better captures DRT peaks due to oxygen transport in channel and GDL[17], while the ORR and higher–frequency peaks are described in a usual way using the Debye kernel.

The characteristic frequency of GDL peak typically exceeds the frequency of channel peak (see below). The frequency f_* of α step is thus taken between the GDL and CCL peaks in order to describe the transport peaks using the K_2 kernel, and the ORR using the standard Debye kernel. Below, the real part of Eq.(5) has been solved using Tikhonov regularization[21] and non–negative least squares (NNLS) solver[22,23]. For all the spectra the Tikhnonov regularization parameter calculated by the L–curve method is $\lambda_T = 3\cdot 10^{-5}$.

IV. RESULTS AND DISCUSSION

The experimental impedance spectra have been calculated from the digitized frequency plots of absolute value $|\mathcal{Z}|$ and phase angle ϕ reported in[16] according to $\mathcal{Z} = |\mathcal{Z}|\exp(\mathrm{i}\phi)$. Mocotéguy et al.[16] published total stack impedance $\mathcal{Z}$ (Ω); from their spectra we calculated impedance Z_{av} of an average cell:

$$Z_{av} = \frac{\mathcal{Z}S_{cell}}{M}, \quad \Omega\ \mathrm{cm}^2 \tag{8}$$

where M is the number of cells in the stack and S_{cells} is the single cell active surface area. The value of $M \simeq 55$ has been determined dividing the static resistivity of the stack by the cell static resistivity measured at the current density of 150 mA cm^{-2}. The value of $S_{cell} = 100$ cm^2 has been taken from the remark on page 16728 of Ref.[16], which states that the current of 1 A corresponds to the current density of 0.01 A cm^{-2}.

A. Fitting spectra

The average cell impedance has been modeled using 6–cell stack with every cell separated into 8 segments. The

spectrum of average cell has been fitted to the experimental spectrum Z_{av}, Eq.(8). Inductance of measuring cables has been taken into account by adding the term $i\omega L_{cab}S_{cell}$ in series with the calculated model impedance. The value of L_{cab} returned by the fitting procedure was $L_{cab} \simeq 1.9 \cdot 10^{-8}$ H regardless of the cell current density. It is worth mentioning that no "external" capacitance[24] was used for spectra fitting. A custom parallel fitting code has been written in Python with MPI library. Calculations have been performed on Intel Xeon–based cluster using 96 cores; fitting of a single stack spectrum takes 2–3 min.

Details of the flow field configuration, in particular channel width/land ratio and channel depth have not been reported in[16]. Fitting has been performed claiming the air flow stoichiometry λ as a fitting parameter. The last row in Table I shows the effective λ_{eff} returned by the fitting procedure. As can be seen, λ_{eff} exceeds $\lambda = 2$ kept in experiment; however, with the growth of stack current, λ_{eff} tends to experimental value. The reason for higher λ_{eff} could to be a pressure drop Δp along a single channel in the cells. To compensate for the loss of air flow velocity due to Δp, the inlet flow rate in experiments could be higher than the one needed in the absence of Δp. Further, the channel depth h in the first (channel) equation in Figure 1 is an effective parameter, which depends on the channel width/rib width ratio. This ratio in unknown and it has been taken equal to 1. More accurate solution to the channel equation requires knowledge of the flow field geometry.

The experimental and fitted model spectra of the average cell in the stack operated at the current densities of 150, 250 and 400 mA cm^{-2} are shown in Figure 2. The dependency of real part of impedance vs frequency is shown in Figure 3. Fitting parameters are listed in Table I. Mean squared residual for the fitted spectra (the last row in Table I) has been calculated as

$$r = \frac{1}{N}\sum_{i=1}^{N}\Big(\big(\mathrm{Re}\,(Z_{exp,i}) - \mathrm{Re}\,(Z_{mod,i})\big)^2 + \big(\mathrm{Im}\,(Z_{exp,i}) - \mathrm{Im}\,(Z_{mod,i})\big)^2\Big) \quad (9)$$

where the subscripts exp and mod mark the experimental and fitted values, N is the total number of points in the spectra. As can be seen, $r \simeq 10^{-5}$ indicates good quality of fitting.

The ORR Tafel slope is around 30 mV/exp (Table I) which is equivalent to about 70 mV/decade, a value well known in literature from kinetic studies[25]. The oxygen diffusion coefficient in the CCL increases by a factor of ten with the cell current density, from $4 \cdot 10^{-4}$ to $45 \cdot 10^{-4}$ cm^2 s^{-1} (Table I). The average value of $15 \cdot 10^{-4}$ cm^2 s^{-1} is close to D_{ox} measured by the Ballard group using Loschmidt cell[26]. Moderate growth of the Tafel slope with the cell current agrees with our previous analysis of single cell spectra[19]. The growth of D_{ox} also agrees with the single–cell results[19]; however, the origin of this growth yet is unclear.

The GDL oxygen diffusivity varying in the range of $6 \cdot 10^{-3}$ to $14 \cdot 10^{-3}$ cm^2 s^{-1} is low, indicating relatively dense GDL used in the Ballard cells. The CCL proton conductivity increasing from 5 to nearly 7 mS cm^{-1} with the cell current (Table I) falls into the range of typical values for the standard Pt/C based electrodes[27,28].

The cell (membrane) ohmic resistance is close to 50 mOhm cm^{-2} and it is independent of cell current (Table I). Note that this value differs from the visible high–frequency intercept of the Nyquist spectrum with the real axis (Figure 2). This is due to effect of cable inductance, which shifts this intercept to higher values.

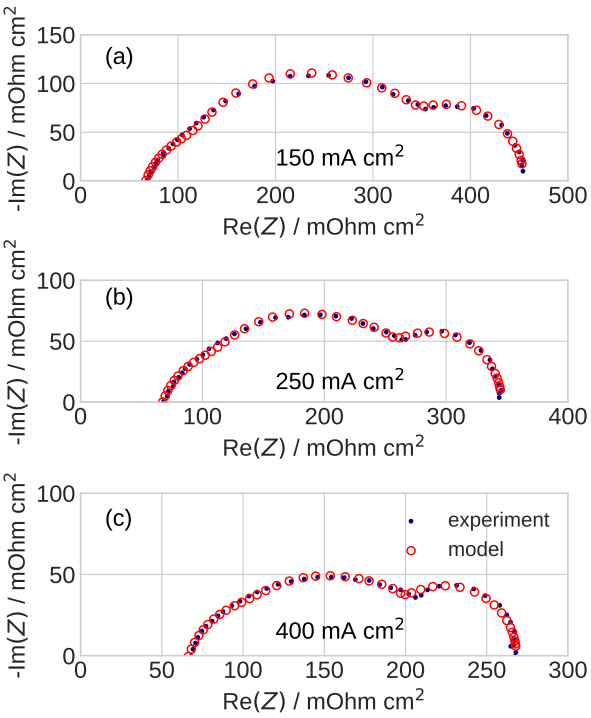

FIG. 2. Experimental (solid points) and fitted model (open circles) Nyquist spectra of an average cell in the stack for the current densities of (a) 150, (b) 250, and (c) 400 mA cm^{-2}.

B. Distribution of relaxation times

Figure 4 shows DRT of the average cell in the stack calculated using the experimental and fitted real parts of impedance. As can be seen, the DRT consists of five peaks, which we attribute to (1) oxygen transport in the channel, (2) oxygen transport in the GDL, (3) oxygen reduction reaction, and (4,5) proton transport. The experimental (Figure 4a) and model (Figure 4b) DRT spectra are very similar giving confidence that the fitted model correctly describes stack impedance.

Figure 5 shows DRT for the stack current densities of 250 and 400 mA cm^{-2}. Figures 4a and 5a,b display evolution of DRT peaks as the stack current increases. The peak

Stack current density / mA cm^{-2}	150	250	400
Tafel slope b / mV/exp	27.5	31.8	34.9
Double layer capacitance C_{dl} / F cm^{-3}	37.0	35.8	38.8
CCL oxygen diffusivity D_{ox} / 10^{-4} cm^2 s^{-1}	4.02	15.5	45.2
CCL proton conductivity σ_p / mS cm^{-1}	5.40	6.05	6.53
GDL oxygen diffusivity D_b / 10^{-4} cm^2 s^{-1}	57.2	89.5	140
Effective air flow stoichiometry λ_{eff}	3.72	3.16	2.85
Ohmic resistance R_{HFR} / mOhm cm^2	49.6	50.6	50.6
Mean squared residual r / 10^{-5}, Eq.(9)	1.17	0.701	0.687

TABLE I. Fitting parameters for the spectra in Figure 2.

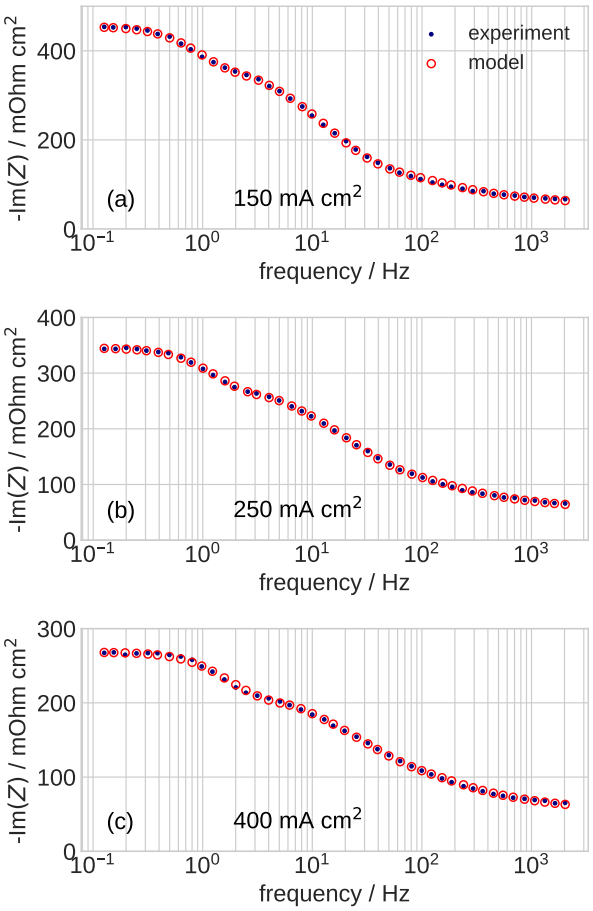

FIG. 3. Experimental (solid points) and fitted model (open circles) frequency dependencies of the real part of an average cell impedance for the current densities of (a) 150, (b) 250, and (c) 400 mA cm^{-2}.

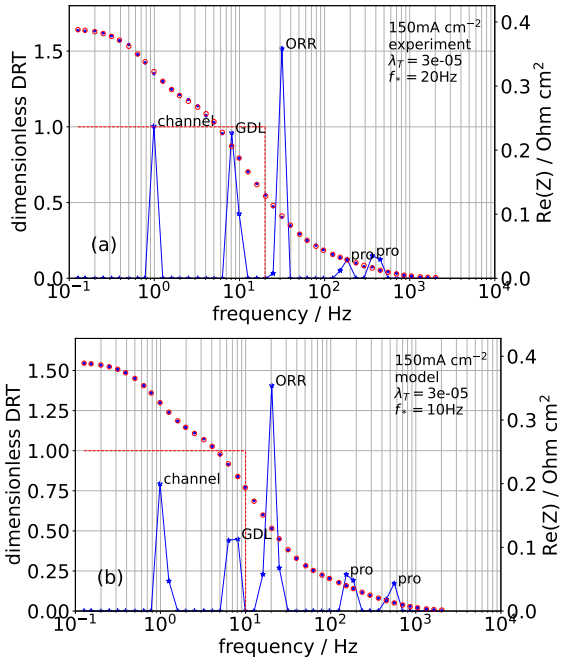

FIG. 4. DRT spectra (solid blue line and stars) calculated using the real part of (a) measured impedance (blue dots) of the Ballard stack and (b) fitted model (Figure 1). Red open circles show the real part of impedance reconstructed from the calculated DRT.

frequencies and resistivities for the three current densities are summarized in Figure 6. The characteristic frequency f_h of channel peak increases from 1 to 2 Hz (Figure 6a). For this frequency, the model[29] gives

$$f_h \simeq \frac{3.3v}{L} \tag{10}$$

where v is the flow velocity in the channel, and L is the channel length. Expressing v from the formula for oxygen stoichiometry λ

$$\lambda = \frac{4Fhvc_h^{in}}{LJ} \tag{11}$$

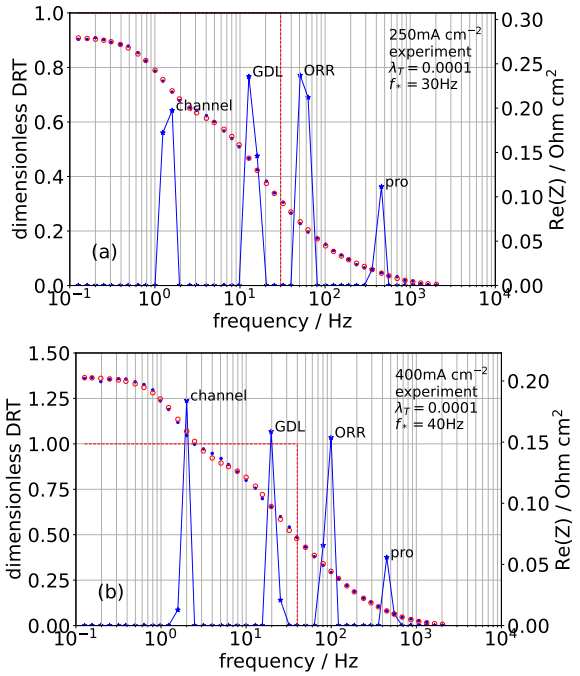

FIG. 5. DRT spectra (solid blue line and stars) calculated using the real part of experimental impedance for the cell currents of (a) 250 and (b) 400 mA cm^{-2}. Red open circles show the real part of impedance reconstructed from the calculated DRT.

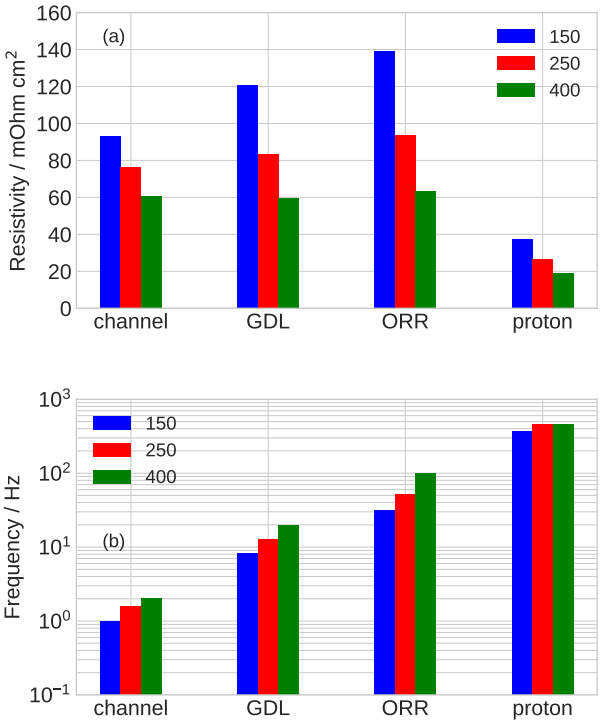

FIG. 6. (a) Peak resistivities and (b) peak frequencies in Figures 4b, 5 for the indicated stack current densities.

and using the result in Eq.(10), we get

$$f_h = \frac{3.3\lambda J}{4Fhc_h^{in}} \tag{12}$$

Here, h is the channel depth, and c_h^{in} is the inlet oxygen concentration. Taking for the estimate $h = 0.1$ cm and the cell operating parameters $J = 0.15$ A cm^{-2}, $c_h^{in} = 6.75 \cdot 10^{-6}$ mol cm^{-3}, $T = 273 + 56$ K, we get $f_h \simeq 3.0$ Hz. Taking into account uncertainty in the channel depth, this value agrees well with the "channel" peak position in Figures 4, 5b. Further, analytical model[30] shows that channel resistivity is inversely proportional to the cell current density. This trend is clearly seen in Figure 5b.

For the characteristic frequency of "GDL" peak (Figure 5b), the Warburg finite–length formula is valid[30]

$$f_{GDL} = \frac{2.54D_b}{2\pi l_b^2} \tag{13}$$

where D_b and l_b are the GDL oxygen diffusivity and thickness, respectively. With $D_b = 0.01$ cm^2 s^{-1} (Table I) and typical value of $l_b = 230 \cdot 10^{-4}$ cm (230 μm), we get $f_{GDL} \simeq 7.6$ Hz, which is close to the average "GDL" peak frequency in Figure 6.

For the ORR peak resistivity (Figure 5a) the following equation holds[31]:

$$R_{ORR} = \frac{b}{J}. \tag{14}$$

With $b = 0.03$ V and J varying from 0.15 A cm^{-2} to 0.4 A cm^{-2}, we get R_{ORR} varying from 0.2 Ohm cm^2 down to 0.075 Ohm cm^2. DRT returns the variation of "ORR" peak resistivity from 0.14 Ohm cm^2 to 0.06 Ohm cm^2, leaving no doubts about the origin of ORR peak. Further, at low current densities the ORR peak frequency is expected to be

$$f_{ORR} \simeq \frac{1}{2\pi R_{ORR} C_{dl} l_t} = \frac{j_0}{2\pi b C_{dl} l_t} \tag{15}$$

For the lowest current density of 150 mA cm^{-2} and the parameters from Table I, we get $f_{ORR} \simeq 23$ Hz, which is close to 30 Hz in Figure 6b.

The last, "proton" peak in Figure 5 describes proton transport in the CCL. It is interesting to note that at the current density of 150 mA cm^{-2}, the proton transport is represented by the double peaks (Figure 4), while at higher currents this doublet merges into a single peak (Figure 5). The second proton peak in Figure 4 could be an artifact due to poor description of proton transport impedance by Debye kernel.

For the characteristic frequency f_p of proton peak, the

following estimate holds[32]

$$f_p \simeq \frac{2\sigma_p}{C_{dl} l_t^2} \tag{16}$$

where σ_p is the CCL proton conductivity and C_{dl} is the electrode volumetric double layer capacitance. Taking for the estimate $\sigma_p = 7 \cdot 10^{-3}$ S cm^{-1} and $C_{dl} = 30$ F cm^{-3} (Table I), we get $f_p \simeq 320$ Hz, in agreement with Figure 6b.

V. CONCLUSIONS

Our recent physics–based model for impedance spectra of a PEM fuel cell has been upgraded to stack level and fitted to measured spectra of a commercial PEMFC stack from Ballard. Fitting returns oxygen and proton transport parameters of an average cell in the stack. The stack experimental spectra have also been used to calculate the distribution of relaxation times (DRT) function. DRT peak positions and resistivities allowed us to estimate the average oxygen and proton transport parameters in the stack. A good agreement between the parameters obtained from the fitted physical model and DRT analysis is demonstrated.

VI. ACKNOWLEDGMENTS

The author acknowledges Forschungszentrum Jülich for support during this work.

[1]Tang, Z., Huang, Q.-A., Wang, Y.-J., Zhang, F., Li, W., Li, A., Zhang, L., and Zhang, J. (2020) Recent Progress in the Use of Electrochemical Impedance Spectroscopy for the Measurement, Monitoring, Diagnosis and Optimization of Proton Exchange Membrane Fuel Cell Performance. *J. Power Sources 468*, 228361.

[2]Huang, J., Gao, Y., Luo, J., Wang, S., Li, C., Chen, S., and Zhang, J. (2020) Editors' Choice–Review–Impedance Response of Porous Electrodes: Theoretical Framework, Physical Models and Applications. *J. Electrochem. Soc. 167*, 166503.

[3]Yuan, X., Sun, J. C., Blanco, M., Wang, H., Zhang, J., and Wilkinson, D. P. (2006) AC Impedance Diagnosis of a 500 W PEM Fuel Cell Stack. Part I: Stack Impedance. *J. Power Sources 161*, 920–928.

[4]Yan, X., Hou, M., Sun, L., Liang, D., Shen, Q., Xu, H., and ans B. Yi, P. M. (2007) AC Impedance Characteristics of a 2 kW PEM Fuel Cell Stack under Different Operating Conditions and Load Changes. *Int. J. Hydrogen Energy 32*, 4358–4364.

[5]Dhirde, A. M., Dale, N. V., Salehfar, H., Mann, M. D., and Han, T.-H. (2010) Equivalent Electric Circuit Modeling and Performance Analysis of a PEM Fuel Cell Stack Using Impedance Spectroscopy. *IEEE Trans. Energy Conv. 25*, 778–786.

[6]Rodat, S., Sailler, S., Druart, F., Thivel, P.-X., Bultel, Y., and Ozil, P. (2010) EIS Measurements in the Diagnosis of the Environment within a PEMFC Stack. *J. Appl. Electrochem. 40*, 911–920.

[7]Mitzel, J., Sanchez-Monreal, J., Garcia-Sanchez, D., Gazdzicki, P., Schulze, M., Häußler, F., Hunger, J., Schlumberger, G., Janicka, E., Mielniczek, M. et al.. (2020) Fault Diagnostics in PEMFC Stacks by Evaluation of Local Performance and Cell Impedance Analysis. *Fuel Cells 20*, 403–412.

[8]Macdonald, D. (2006) Reflections on the History of Electrochemical Impedance Spectroscopy. *Electrochim. Acta 51*, 1376–1388.

[9]Canut, J.-M. L., Abouatallah, R. M., and Harrington, D. A. (2006) Detection of Membrane Drying, Fuel Cell Flooding, and Anode Catalyst Poisoning on PEMFC Stacks by Electrochemical Impedance Spectroscopy. *J. Electrochem. Soc. 153*, A857–A864.

[10]Fuoss, R., and Kirkwood, J. (1941) Electrical Properties of Solids. VIII. Dipole Moments in Polyvinyl Chloride-Diphenyl Systems. *J. Am. Chem. Soc. 63*, 385–394.

[11]Schichlein, H., Müller, A. C., Voigts, M., Krügel, A., and Ivers-Tiffée, E. (2002) Deconvolution of Electrochemical Impedance Spectra for the Identification of Electrode Reaction Mechanisms in Solid Oxide Fuel Cells. *J. Appl. Electrochem. 32*, 875–882.

[12]Heinzmann, M., Weber, A., and Ivers-Tiffée, E. (2018) Advanced Impedance Study of Polymer Electrolyte Membrane Single Cells by Means of Distribution of Relaxation Times. *J. Power Sources 402*, 24 – 33.

[13]Reshetenko, T., and Kulikovsky, A. (2020) Distribution of Relaxation Times: A Tool for Measuring Oxygen Transport Resistivity of a Low–Pt PEM Fuel Cell Cathode. *J. Electrochem. Soc. 167*, 144505.

[14]Cohen, G. A., Gelman, D., and Tsur, Y. (2021) Development of a Typical Distribution Function of Relaxation Times Model for Polymer Electrolyte Membrane Fuel Cells and Quantifying the Resistance to Proton Conduction within the Catalyst Layer. *J./ Phys./Chem./ C 125*, 11867–11874.

[15]Wang, Q., Hu, Z., Xu, L., Gan, Q., 1, J. L., Du, X., and Ouyang, M. (2021) A Comparative Study of Equivalent Circuit Model and Distribution of Relaxation Times for Fuel Cell Impedance Diagnosis. *Int. J. Energy Res. 45*, 15948–15961.

[16]Moçotéguy, P., Ludwig, B., Beretta, D., and Pedersen, T. (2021) Study of the Impact of Water Management on the Performance of PEMFC Commercial Stacks by Impedance Spectroscopy. *Int. J. Hydrogen Energy 45*, 16724–16737.

[17]Kulikovsky, A. (2021) A Kernel for PEM Fuel Cell Distribution of Relaxation Times. *Front. Energy Res. 9*, 780473.

[18]Kulikovsky, A., and Shamardina, O. (2015) A Model for PEM Fuel Cell Impedance: Oxygen Flow in the Channel Triggers Spatial and Frequency Oscillations of the Local Impedance. *J. Electrochem. Soc. 162*, F1068–F1077.

[19]Reshetenko, T., and Kulikovsky, A. (2016) Variation of PEM Fuel Cell Physical Parameters with Current: Impedance Spectroscopy Study. *J. Electrochem. Soc. 163*, F1100–F1106.

[20]Chang, P. A., St-Pierre, J., Stumper, J., and Wetton, B. (2006) Flow distribution in proton exchange membrane fuel cell stacks. *J. Power Sources 162*, 340–355.

[21]Tikhonov, A. N. *Numerical Methods for the Solution of Ill-Posed Problems*; Kluwer: Dordrecht, 1995.

[22]Kulikovsky, A. (2020) PEM Fuel Cell Distribution of Relaxation Times: A Method for Calculation and Behavior of Oxygen Transport Peak. *Phys. Chem. Chem. Phys. 22*, 19131–19138.

[23]Kulikovsky, A. (2021) Impedance and resistivity of low–Pt cathode in a PEM fuel cell. *J. Electrochem. Soc. 168*, 044512.

[24]Reshetenko, T., and Kulikovsky, A. (2019) On the Origin of High Frequency Impedance Feature in a PEM Fuel Cell. *J. Electrochem. Soc. 166*, F1253–F1257.

[25]Liu, Y., Murphy, M. W., Baker, D. R., Gu, W., Ji, C., Jorne, J., and Gasteiger, H. A. (2009) Proton Conduction and Oxygen Reduction Kinetics in PEM Fuel Cell Cathodes: Effects of Ionomer-to-Carbon Ratio and Relative Humidity. *J. Electrochem. Soc. 156*, B970–B980.

[26]Shen, J., Zhou, J., Astrath, N. G. C., Navessin, T., Liu, Z.-S. S., Lei, C., Rohling, J. H., Bessarabov, D., Knights, S., and Ye, S. (2011) Measurement of Effective Gas Diffusion Coefficients of Catalyst Layers of PEM Fuel Cells With a Loschmidt Diffusion Cell. *J. Power Sources 96*, 674–678.

[27]Liu, Y., Gu, W., Baker, D. R., Jorne, J., and Gasteiger, H. A. (2010) Proton Conduction in PEM Fuel Cell Cathodes: Effects of Electrode Thickness and Ionomer Equivalent Weight. *J. Electrochem. Soc. 157*, B1154–B1162.

[28]Liu, Y., C.Li,, Gu, W., Jorne, J., and Gasteiger, H. A. (2011) Effects of Catalyst Carbon Support on Proton Conduction and Cathode Performance in PEM Fuel Cells. *J. Electrochem. Soc. 158*, B614–B621.

[29]Kulikovsky, A. (2019) Analytical Impedance of Oxygen Transport in a PEM Fuel Cell Channel. *J. Electrochem. Soc. 166*, F306–F311.

[30]Kulikovsky, A. (2021) Analytical Impedance of Oxygen Transport in the Channel and Gas Diffusion Layer of a PEM Fuel Cell. *J. Electrochem. Soc. 168*, 114520.

[31]Reshetenko, T., and Kulikovsky, A. (2015) PEM Fuel Cell Characterization by Means of the Physical Model for Impedance Spectra. *J. Electrochem. Soc. 162*, F627–F633.

[32]Kulikovsky, A. (2020) Analysis of Proton and Electron Transport Impedance of a PEM Fuel Cell in H_2/N_2 regime. *Electrochem. Sci. Adv. e202000023*.

Nomenclature

$\tilde{}$	Marks dimensionless variables
b	ORR Tafel slope, V
C_{dl}	Double layer volumetric capacitance, F cm^{-3}
c_b	Oxygen molar concentration in the GDL, mol cm^{-3}
c_h	Oxygen molar concentration in the channel, mol cm^{-3}
c_h^{in}	Reference (inlet) oxygen concentration, mol cm^{-3}
D_b	Oxygen diffusion coefficient in the GDL, cm^2 s^{-1}
D_{ox}	Oxygen diffusion coefficient in the CCL, cm^2 s^{-1}
F	Faraday constant, C mol^{-1}
f	Frequency, Hz
h	Cathode channel depth, cm
i_*	ORR volumetric exchange current density, A cm^{-3}
i	Imaginary unit
J	Mean cell current density, A cm^{-2}
j	Local proton current density in the CCL, A cm^{-2}
L	Cathode channel length, cm
L_{cab}	Cable inductance, H
l_b	GDL thickness, cm
l_t	CCL thickness, cm
M	Number of cells in the stack
N	Number of segments in a cell
R_∞	High–frequency cell resistivity Ω cm^2
R_{pol}	Polarization cell resistivity Ω cm^2
S_{cell}	Cell active area, cm^2
t	Time, s
v	Flow velocity in the cathode channel, cm s^{-1}
x	Coordinate through the cell, cm
y	Distance along the manifold for air supply
Z	Impedance, Ohm cm^2
Z_{cell}	Single cell impedance, Ohm cm^2
Z_{seg}	Segment impedance, Ohm cm^2
Z_{stack}	Stack impedance, Ohm cm^2
$\mathcal{Z}_{stack}$	Total stack impedance, Ohm
z	Coordinate along the cathode channel, cm

Subscripts:

b	In the GDL
f	faradaic
h	Air channel
p	Proton

Greek:

α	Step function, Eq.(6)
η	ORR overpotential, positive by convention, V
λ	Air flow stoichiometry, Eq.(11)
λ_T	Tikhonov regularization parameter
ϕ	Phase angle of $\mathcal{Z}$, radians
σ_p	Proton conductivity of the CCL, S cm^{-1}
τ	Time constant, Eq.(5)
ω	Angular frequency of the AC signal, s^{-1}